2020 IEEE/RSJ International Conference on Intelligent Robots and Systems (IROS)
October 25-29, 2020, Las Vegas, NV, USA (Virtual)

Towards the Development of a Robotic Transcatheter Delivery System for Mitral Valve Implant

Namrata Nayar*, Seokhwan Jeong and Jaydev P. Desai, *Fellow IEEE*

***Abstract*— Mitral regurgitation is one of the most common heart diseases caused by ventricular dysfunction or anatomic abnormality of the mitral valve. The fundamental treatment for mitral regurgitation is to repair/replace the mitral valve through open-heart surgery which is risky and requires more time to recover or through minimally invasive approaches, which have significant challenges and limitations. Through the transcatheter approach, the mitral valve implant is minimally invasively delivered directly to the mitral valve and is clamped onto the leaflet to mitigate or prevent regurgitation. However, this procedure requires delicate manipulation of the catheter in a constrained space and remains a challenging problem. In this work, we present a robotically steerable cathether design for the transcatheter procedure to address mitral regurgitation. The proposed catheter consists of two bending joints, one torsion joint, and implant delivery module at the distal end of the robot. Kinematic models for each joint design are derived and compared with experimental results. Finally, we experimentally demonstrate the feasibility of the proposed catheter to navigate in a phantom heart model. In this demonstration, the bending joint was actuated by 75°, the torsion joint was actuated by 90° and the implant was pushed out by 1.8 mm to deliver the implant.**

I. Introduction

Mitral regurgitation (MR) is the most common form of valvular heart disease (VHD) in the United States and is caused due to the leakage of blood (i.e., back flow from the left ventricle to the left atrium) through the mitral valve every time the left ventricle contracts [1]. The heart valves ensure the flow of blood in one direction and prevent the back-flow during systole and diastole. Mitral regurgitation (MR) leads to an increase in pressure in the left atrium and left ventricular dilatation and progressively to congestive heart failure and death. It is caused by ventricular dysfunction or anatomic abnormality of the mitral valve. 1.7 % of US adult population and 9.3 % of adults over 75 years suffer from MR [2], [3] and the mortality rate of patients with MR can increases up to 57 % if proper treatment is not provided [4]. Medications can be prescribed to relieve symptoms arisen from MR, however, it is optimal to physically repair/replace the mitral value by suturing leaflets or implanting an artificial ring through an open-heart surgery. Minimally invasive approaches for mitral valve surgery have been pioneered along with advancements in imaging, surgical instrumentation, and robotic technology during the past 20 years [5] to reduce morbidity, postoperative pain, and time to return to normal activity from open-heart surgery [6], [7]. More recently, transcatheter mitral valve repair/replacement approaches through percutaneous procuredures have been developed for MR treatment that involves implanting a 'clip' on the mitral valve [8]. One example is the FDA approved transcatheter intervention utilizing the MitraClip® system [9]. A steerable catheter delivers the clip and reshapes the mitral valve by clamping the leaflets together. In this procedure, a clinician manually navigates the catheter by bending/torquing the distal part. While this transcatheter approach is gaining traction, maneuverability of the tip whereby it does not adversely affect surrounding anatomy such as entanglement in chrodae tendineae and obstruction of ventricular outflow tract remains a clinical challenge [8], [10]. Currently, most off-the-shelf catheters are manually operated and have limited range of motion; Its operation relies a lot on the operators' skill and experience [11]. Steerability by manual and/or external actuators allows the operator to have improved catheter maneuverability and accessibility to target regions.

For precise clip implantation during MR treatment through the transcatheter approach, the clip must be aligned in proper orientation depending on the shape of the mitral valve [12], [13]. Therefore, the torsion and bending capability are critical factors to provide successful deployment of the clip on the mitral valve leaflet. Commercially available robotically steerable cathethers have shown poor torque transmission efficiency [14] and no direct torsion capability of the distal tip. The MitraClip® does provides rotary motion of the clip, but is remotely operated through a long torque transmission line at the back end, which may not directly control the clip.

In this paper, we present a preliminary design of a robotically steerable catheter with direct torsion and bending joints for effective manipulation of the mitral valve implant clip (i.e., Cardiac Leaflet Enhancer [15]) to provide efficient MR treatment and management of the disease. The proposed robotic catheter has two bending joints, one torsion joint, and one implant module at its distal end. This paper is organized as follows: Section II introduces the design and kinematics for each actuation joint of the proposed robot. Section III contains experiments performed on each joint and compares the theoretical and experimental results to validate the theory developed in section II. It also covers the demonstration of the proposed robot in a phantom heart model. Finally,

Research reported in this publication was supported in part by the National Heart, Lung, And Blood Institute of the National Institutes of Health under Award Number R01HL140325. The content is solely the responsibility of the authors and does not necessarily represent the official views of the National Institutes of Health.

N. Nayar, S. Jeong, and J. P. Desai are with the Medical Robotics and Automation (RoboMed) Laboratory, Georgia Center for Medical Robotics (GCMR), Wallace H. Coulter Department of Biomedical Engineering, Georgia Institute of Technology, Atlanta, GA, USA.

*N. Nayar is the corresponding author {nnayar7@gatech.edu}.

discussion and conclusion are provided in Section IV.

II. Robot Design and Kinematics

To deploy the implant on the mitral valve, a catheter containing the implant should be introduced into the left atrium from the right atrium through a transseptal puncture of the interatrial septum, which is a well established clinical procedure [16]. Once the catheter is introduced and maneuvered to the right orientation, the implant at the distal tip is pushed through the mitral valve opening and clamps on the mitral valve leaflet with delicate manipulation.

To implement this procedure, we propose a steerable catheter consisting of four tendon-driven units: two bending joints, one torsion joint, and one implant delivery module (IDM). Each bending joint is controlled by two antagonistic tendons and the two bending joints are designed to have low coupling. The torsion joint provides direct torsion motion to the IDM, thereby providing better manipulability than the existing torsion mechanisms operated at the back end in current clinical practice. Furthermore, the joint has been designed to have a wide hollow lumen to effectively accommodate the implant, hence reducing the length of the robot and protecting the implant from exposure to its surroundings. The detailed design and mechanism of each component is presented in the following subsections.

A. Design of Bending Joint

The bending joint consists of a top disk and a bottom disk that are connected by a spring introduced in [17] (see Fig. 1). The ability of a spring to bend laterally provides the compliance required for bending motion. By varying the dimensions of the spring (i.e., coil diameter, pitch, and radius), the overall stiffness of the spring can be changed. Control over this attribute is essential to: (1)maximizing the compliance of the bending joint, and (2)minimizing the coupling between the bending and torsion joints by using a stiffer bending joint.

For each bending joint, the two nylon tendons are attached to the top disk at diametrically opposite points (see A_1 and A_2 in Fig. 1 (a)), routed through the inner passages in the bottom disk (see B_1 and B_2 in Fig. 1 (a)), and led to the hollow inner lumen of the robot (see Fig. 1 (b)). Fig. 1(a) shows the geometry of an actuated bending joint. Here, it is assumed that the length of the arc passing through the contact points of the spring on the bending side, S, retains its length since it is 3D-printed as a tension spring. The arc connecting the centers of the top and bottom disk, $\widehat{\mathrm{A'\,B'}}$, varies in length as the bending angle, θ, changes. Here, the coordinates of A′ and B′ are: $((r+R)(1-\cos(\theta)), 0, (r+R)(\sin(\theta)))$ and $(0,0,0)$, respectively. Thus, the length of the chord $\widehat{\mathrm{A'\,B'}}$, namely L_c is given by:

$$L_c = 2(r+R)^2(1-\cos(\theta)) \tag{1}$$

where r and R are the radius of the spring and the radius of curvature of the arc subtended by S respectively. Since $\widehat{\mathrm{A_1B_1}}$ is part of the circle with radius $R-\delta$, the relationship between the bending angle, θ, and the tendon displacement,

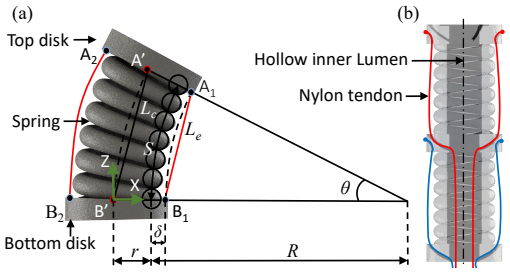

Fig. 1: Schematic of the bending joint: (a) Actuated state, (b) Cross-section of the joint.

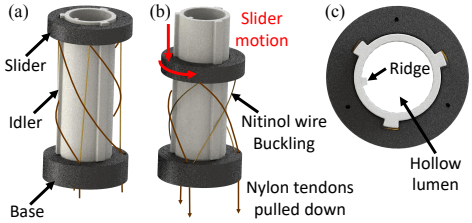

Fig. 2: Schematic of the torsion joint depicting : (a) the 3 units at rest (home position), (b) the nitinol wire buckling when the nylon tendons are pulled causing the slider to translate and rotate, and (c) the top view.

L_k, is given by:

$$L_k = S - L_e = S - 2(R-\delta)^2(1-\cos(\theta)) \tag{2}$$

In theory, the desired θ should be achieved by the pure kinematic relationship from Eq.2; however, we observed that in practice, the total tendon displacement, L_t is dominated by tendon elongation due to the high stiffness of the spring. Therefore, L_t, is the summation of L_k and the elongation caused by tension and is expressed as:

$$L_t = L_k + \frac{K_s\theta}{k_n} \tag{3}$$

where K_s and k_n are the lateral stiffness of the spring and linear stiffness of the nylon tendon respectively, which are derived from experiments in section III-B.

B. Design of Torsion Joint

To implement torsion motion of the implant to align with the mitral leaflets, we designed a new type of torsion mechanism. The torsion joint consists of three units: a slider, an idler, and a base as shown in Fig. 2(a). The base is rigidly fixed to the end of the top disk (see Fig. 1(a)) of the bending joint. The slider and base are held apart by three flexible and superelastic Nitinol wires located 120° apart circumferentially. Minimum three wires are necessary to keep the slider parallel to the base at all times. Moreover, three nylon tendons attached to the slider, each 120° apart, wrap around the idler and pass through holes in the base, finally reaching the hollow lumen. When these tendons are pulled together, the slider moves down, forcing the Nitinol wires to buckle (see Fig 2(b)), which results in simultaneous rotation and translation of the slider with respect to the base like a screw motion. Here, the idler is free to rotate with respect to the base, therefore, the screw motion of the slider coupled with the idler through a prismatic joint makes a pure rotational motion of the idler. Simultaneously, since the inner ridge along the hollow lumen (i.e., male part, see Fig. 2(c)) of the idler engages with the groove in the implant holder

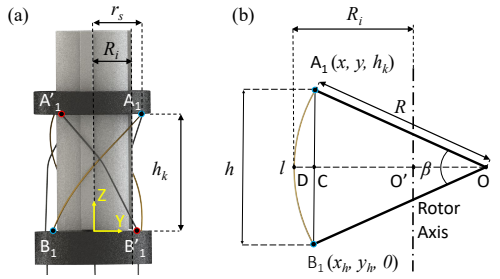

Fig. 3: (a) Torsion joint in actuated state and, (b) schematic of the Nitinol tendon with essential dimensions and geometric relations.

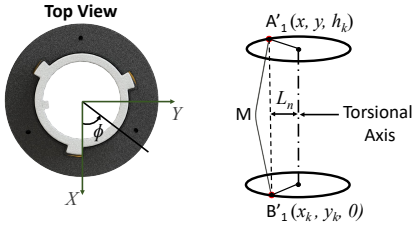

Fig. 4: Top view of the torsion joint to visualize the angular displacement and the schematic of a taut nylon tendon. Here, at the point M, the nylon thread grazes over the Idler.

(i.e., female part) of the IDM, the rotational motion of the idler is finally coupled with the implant holder and rotates it to the target orientation.

Fig. 3 and Fig. 4 provide geometric relationships between tendon displacement and the angular motion of the slider. Here $\mathrm{A}_1(x, y, h_k)$ and $\mathrm{B}_1(x_h, y_h, 0)$ represent the coordinates of the Nitinol wire housing points on the slider and base, respectively. $\mathrm{A}'_1(x, y, h_k)$ and $\mathrm{B}'_1(x_k, y_k, 0)$ represent the coordinates of nylon tendon attachment points in the slider and the hole in the base, respectively, while r_s is the distance between the tendon attachment point on the slider and the axis of the torsion joint. The point A_1 rotates with respect to the axis of the torsion joint along the circle of radius r_s and the relationship is given by:

$$x^2 + y^2 = r_s^2 \tag{4}$$

Here, we assume that the Nitinol wires have constant curvature during the motion of the slider, then the shape of the wire can be projected on the plane passing through A_1, B_1, and O with an arc shape. (see Fig. 3 (b)). From the geometric relationship in Fig 3 (b), we can derive following equations:

$$h = \sqrt{(x - x_h)^2 + (y - y_h)^2 + h_k^2} \tag{5}$$

$$\sin\left(\frac{\beta}{2}\right) = \frac{h}{2R}; \qquad \beta = \frac{l}{R} \tag{6}$$

where β is the angle subtended by the curved Nitinol wire, h is the chord of $\overset{\frown}{\mathrm{A}_1\mathrm{B}_1}$, R is the radius of curvature of the Nitinol wire, and l is the length of Nitinol wire.

Since the Nitinol wires are displaced just enough to minimize the strain energy, the wires always stay in contact with the idler at point D to have minimum curvature. From this geometric constraint, the summation of length of $\overline{\mathrm{DC}}$ and $\overline{\mathrm{CO}'}$ should be the same as radius of the idler, R_i. The constraint equation is expressed as follows:

$$R_i = R\left(1-\cos\left(\tfrac{\beta}{2}\right)\right) + \sqrt{\left(\tfrac{x+x_h}{2}\right)^2 + \left(\tfrac{y+y_h}{2}\right)^2} \tag{7}$$

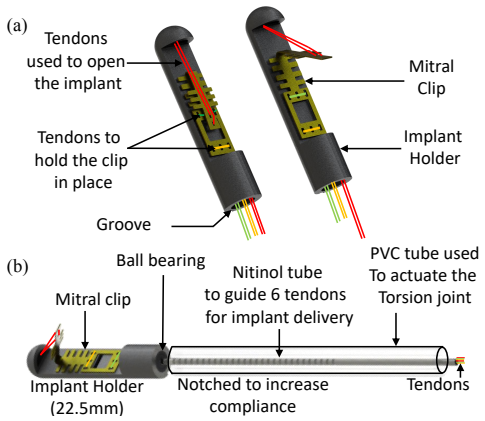

Fig. 5: Schematic of: (a) implant closed and opened by tendon manipulation and (b) entire implant delivery module.

Eqs. 4-7 (i.e., 5 equations) have 5 unknowns: β, R, h, x, and y. We are interested in x and y, as these parameters lead to the tendon displacement and the angle by which the torsion joint rotates. However, to solve the equation, we isolate β and then back-substitute its value into Eqs. 4- 7 to obtain x and y. In Eq. 8, all the variables other than β and h_k are known and we obtain the relationship between β and h_k as:

$$\left[2R_i - \tfrac{2l}{\beta}\left(1-\cos\left(\tfrac{\beta}{2}\right)\right)\right]^2 - 4r^2 - h_k^2 + \left(\tfrac{2l}{\beta}\sin\left(\tfrac{\beta}{2}\right)\right) = 0 \tag{8}$$

Once β is calculated for a given h_k, we can solve for x and y. Consequently, the angle of rotation, ϕ, of the slider with respect to the base can be calculated once x and y are known through the relation: $\phi = \arctan 2(y, x)$, which takes into consideration the x and y values and the quadrant in which these values lie.

Since the nylon tendon is geometrically restricted by the idler, the tendon length between the slider and base was calculated by finding the sum of lengths of $\overline{\mathrm{A}'_1\mathrm{M}}$ and $\overline{\mathrm{MB}'_1}$ which are segments of the tendon (see Fig. 4). Let L_n be the shortest distance between the line $\overline{\mathrm{A}'_1\mathrm{B}'_1}$ and the torsion axis. Then, the point M is observed to be: $(\frac{x-x_k}{2}\frac{R_r}{L_n}, \frac{x-x_k}{2}\frac{R_r}{L_n}, \frac{h_k}{2})$, where $x_k = x_h + r\cos(\frac{4}{3}\pi)$ and $y_k = y_h + r\sin(\frac{4}{3}\pi)$. For a given h_k, we can now calculate the angular displacement of the slider and the nylon tendon displacement. It is important to note that a constant curvature assumption has been made for the Nitinol wire in the model, whereas in reality that holds only if the Nitinol wire had a spherical joint with respect to the slider and base. In our model for a robust and durable design, the tendon is attached rigidly and hence only a majority of the Nitinol wire follows the constant curvature assumption.

C. Delivery system for the implant

As shown in Fig. 5(a), the IDM consists of: a 3D printed implant holder, the mitral implant [15], a ball bearing, and a unidirectionally notched Nitinol tube (Confluent Medical, California, USA) with an outer diameter of 0.889 mm. The Nitinol tube is laser cut (Optec Laser S.A., Frameries, Belgium) to create notches, which increases the compliance of the tube and the entire assembly. The tube is connected to the implant holder with a bearing. The IDM is finally

assembled into the hollow lumen of the proposed catheter. Six tendons from the implant holder pass through the Nitinol tube and manipulate the mitral clip. Holding four of the tendons steady (two of green and yellow tendons in Fig. 5(a)), pulling/releasing the other two (red tendons in Fig. 5(a)) opens/closes the implant. Due to the ball bearing, the motion of the Nitinol tube is decoupled from the rotary motion of implant holder actuated by the torsion joint (thereby making it possible to align the notches of the tube with the direction of bending).

D. Prototype of the Robot

As shown in Fig. 6 (a), the outer part of the steerable catheter is comprised of two bending joints and one torsion joint. The three segments are 3D printed together. The maximum diameter of the entire unit is 10 mm. To assemble the torsion joint, three Nitinol wires of length 20 mm and outer diameter (OD) 200 μm are used. To actuate the bending and torsion joints, nylon tendon of OD 200 μm is used. The three nylon tendons from the torsion joint are attached to a PVC tube, concentrically aligned with the Nitinol tube, (see Fig. 5) 120° apart. To assemble the bending joint, we attach the nylon tendon to the top disk and pass it through a passage in the bottom disk such that it reaches the hollow lumen and minimizes coupling between the two bending joints. Also we use PTFE tubing to ensure smooth movement of the tendons through the passages. The other important parameters include S, r, δ, R_i, and l, which are 12 mm, 3.2 mm, 1 mm, 3.2 mm, and 18 mm, respectively.

The steerable catheter and the IDM are assembled individually (see Fig. 6(b)). The IDM is inserted into the 5 mm inner diameter (ID) hollow lumen of the steerable catheter from the top. It is ensured that the 0.889 mm Nitinol tube passes through the PVC tube of 1.5 mm ID and 3 mm OD. The implant holder of 4.7 mm OD is accommodated inside the 5 mm ID hollow lumen of the torsion joint. The groove on the implant holder engages with the ridge on the idler of the torsion joint, which results in linear motion of the holder with respect to the idler, thereby making it possible to align the implant. Due to a bearing between the implant holder and the Nitinol tube (see Fig. 5(b)), the rotary and the linear motion of the IDM are independently controlled by the torsional joint and the Nitinol tube, respectively. Fig. 6(c) demonstrates rotation of the implant holder and Fig. 6(d) demonstrates linear motion of the IDM and opening of the clip.

III. Experiment

A. Actuation system

Fig. 7 shows the actuation system used to actuate the proposed steerable catheter. A pair of nylon tendons are connected to each bending joint for antagonistic motion and PVC tube is connected to the torsion joint via the three nylon tendons. Each nylon tendon was selectively connected and actuated by linear actuators (Maxon Precision Motors) for each experiment. The controller was designed and operated in Simulink (MATLAB 2019a, The Mathworks Inc.). Rollers

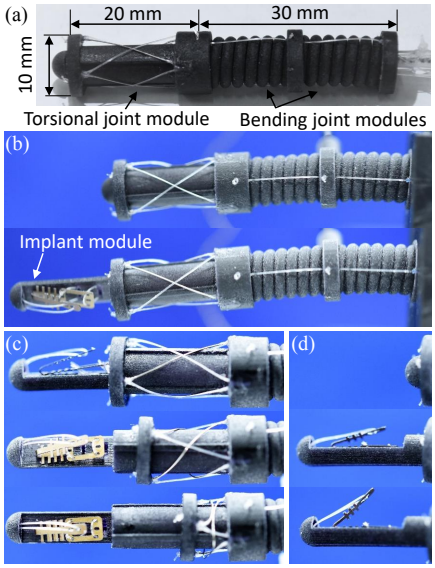

Fig. 6: (a) Assembled catheter including IDM, (b) Implant module retracted in and pushed out, (c) Torsion joint manipulating the angle of the implant holder, and (d) Mitral clip opened and closed.

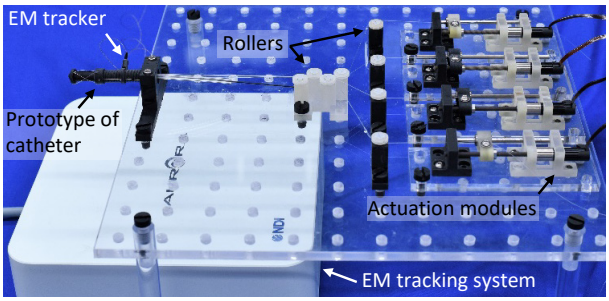

Fig. 7: Experimental setup.

between the catheter and actuators provide a consistent path for the tendons. The bending and torsion angles of each joint were obtained from an electromagnetic (EM) tracking system (Northern Digital Inc. Medical Ontario).

B. Bending joint

This experiment consists of three parts: 1) Estimating the stiffness of the nylon tendon and 2) the lateral stiffness of the 3D-printed spring, and 3) comparing the theoretical and experimental values of the relationship between the bending angle and tendon displacement.

In the first experiment, one end of the nylon tendon was attached to a rigid support and the other end was connected to a force sensor (MDB-5, Transducer Techniques) actuated by the linear motor. The displacement was obtained from the encoder signal of the motor and the force sensor provided the force values. Fig. 8(a-i) shows the results of the experiment. The stiffness of the nylon tendon, k_n, was calculated to be 1.45 N/mm by finding the slope of the best fit line during the loading phase.

In the second experiment, the bending joint was attached to a 3D-printed holder and one of the proximal nylon tendons was connected to the bending joint and pulled by the linear motor. The bending angle of the top disk was recorded using an EM tracker. Fig. 8(a-ii) shows the result of the experiment. The lateral stiffness of the spring, K_s, was calculated to be

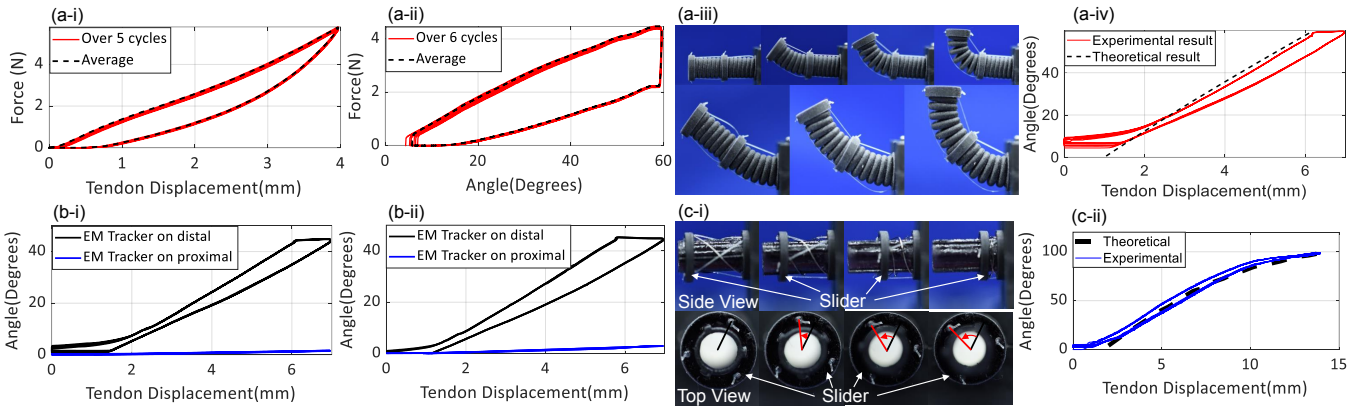

Fig. 8: Results from the experiments: (a-i) Nylon tendon stiffness test, (a-ii) Bending joint lateral stiffness test (a-i) Image of the distal bending joint at various stages of actuation when the proximal joint angle is held at $0°$ and $45°$ respectively, and (a-iv) Comparison of the theoretical and experimental results for the relationship between the bending angle and tendon displacement of the bending joint. Coupling between bending joints when proximal angle is held at (b-i) $0°$, and (b-ii) $45°$. (c-i) Images of the torsion joint taken at different stages of actuation: side view and top view, and (c-ii) Comparison of the theoretical model and experimental results for the relationship between the rotational angle and tendon displacement of the torsion joint

0.076 N/degree by finding the slope of the best fit line during the loading phase. Fig. 8(a-iii) (top) depicts lateral bending of the distal joint while the proximal bending joint is held stationary.

In the last experiment, we obtain the resultant graph between the tendon displacement and the bending angle (see Fig. 8(a-iv)). The theoretical values (black dashed lines) were calculated using Eq. 3 with the measured k_n and K_s from the previous experiments. The theoretical model compared well with the experimental data. In the experiments explained above, results are collected over 5-6 cycles to ensure repeatability of the bending joint. However, each actuation cycle lasted for 10 secs to ensure that it regained it's initial state. Using a material with better elasticity will be part of our future work.

C. Coupling between bending joints

In this experiment, we investigate the amount of coupling between the two bending joints. The four actuation modules shown in Fig. 7 were used to control the nylon tendons attached to the bending joints. For the first experiment, we held the proximal joint at $0°$ (proximal tendons under tension), and actuated the distal joint to $45°$. In the next experiment, we held the proximal joint at $45°$, and actuated the distal joint to $45°$ (see Fig. 8(a-iii) (bottom)). The bending angle values of the distal and proximal joint were obtained from the EM trackers attached to each joint.

In Figs. 8(b-i) and 8(b-ii), the black lines correspond to the angles by which the distal joint bends and the blue lines correspond to the change in the proximal joint angle. In an ideal situation, the proximal joint angle should be unaffected by distal actuation. From the graphs, it is seen that a small deflection of $0°$-$2°$ and $3°$-$4°$ occurs, when the initial proximal joint angle is $0°$ and $45°$, respectively, which is negligible compared to the bending angle of the distal joint.

D. Torsion joint

In this experiment, the base of the torsion joint was attached to a 3D printed holder and the tendon connected to the joint was pulled by the linear actuator (see Fig. 8(c-i)). Achieving forward and reverse motion of $45°$ was set for proper manipulation of the mitral implant. Fig. 8(c-ii) shows the comparison between the experimental result and the theoretical model derived in Section. II-B. The torsion joint can twist slightly more than 90 degrees in one direction thereby achieving the required range of motion.

E. Demonstration of implant delivery in a phantom heart model

To demonstrate the motion of the robotically steerable catheter, it was introduced into a 3D-printed phantom heart model with an artificial leaflet made of silicone (see Fig. 9). The robot was fixed on the phantom heart model at almost the same location where the transseptal puncture is performed. This is implemented on the interatrial septum, which is known as an optimal puncture location for transcatheters [12], [18]. To deliver the clip onto the target leaflet, the following steps were adopted: 1) Bend the distal bending joint by $45°$ followed by the proximal bending joint by $30°$, 2) Push out the implant holder by controlling the notched Nitinol tube, 3) Rotate the implant holder by actuating the torsion joint such that it is aligned with the Mitral valve leaflet, 4) Push the implant holder further to get the implant below the valve, 5) Open the clip as shown in Fig. 5(a), and 6) Position the clip to clamp on the leaflet by fine manipulation. The bending of the first two joints were actuated with the help of linear motors and the remaining steps were performed manually. First, the bending joint was actuated by $75°$, then the torsion joint was actuated by $90°$ and finally the implant was pushed out by 1.8 mm to deliver the implant. This demonstration shows the feasibility of the proposed design for robotic transcatheter delivery of the implant. However, we observed coupling between the torsion and bending joints which can be resolved by using an alternate material with lower friction than PVC. Moreover, the outer diameter, currently 10 mm, should be reduced to 8 mm to be clinically relevant in our future work, referring the state-of-the-art guide catheter diameter (i.e., 8 mm) for MitralClip® [9]. Additionally, automating

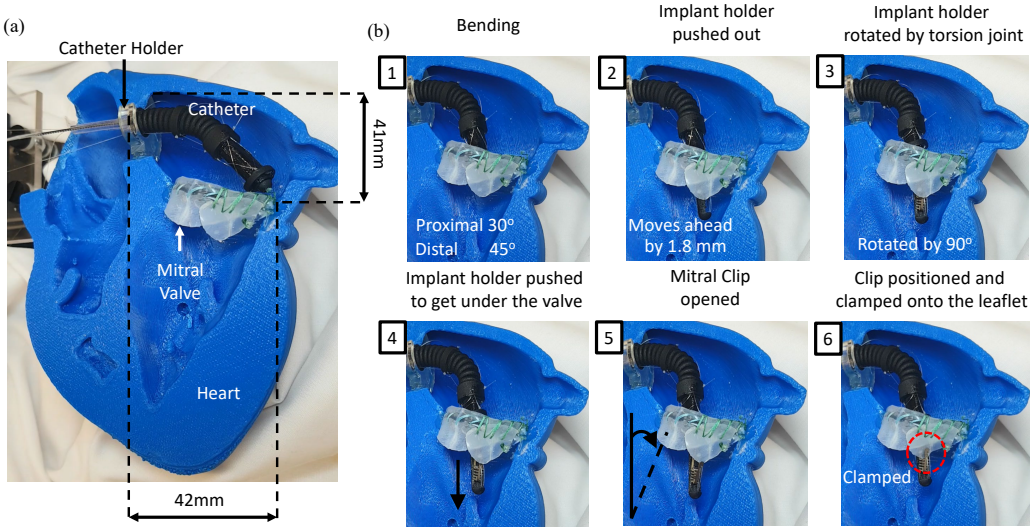

Fig. 9: (a) Demonstration of the transcatheter intervention with a phantom heart model; (b) Procedure to deliver the implant to the mitral valve leaflet.

the entire procedure will remedy finer manipulation of the proposed catheter in our future works.

IV. Conclusions and Future Work

In this work, we proposed a robotically steerable catheter design and development for the transcatheter intervention procedure to treat mitral regurgitation. The proposed design has two bending joints with low inter joint coupling and one directly actuated torsion joint. The kinematic models for each joint was derived and compared with experimental results. Finally, the transcatheter procedure was demonstrated with the proposed catheter containing an implant delivery module. In our future work, we will work towards implementing a fully automated actuation system and perform navigation under ultrasound guidance.

References

[1] M. P. R. J. Moore M, Chen J, "The direct health-care burden of valvular heart disease: Evidence from US national survey data," *Clinicoecon Outcomes Res.*, vol. 8, pp. 613—-627, 2016.

[2] D. Mozaffarian, E. J. Benjamin, A. S. Go, D. K. Arnett, M. J. Blaha, M. Cushman, S. R. Das, S. De Ferranti, J.-P. Després, H. J. Fullerton *et al.*, "Executive summary: heart disease and stroke statistics—2016 update: a report from the american heart association," *Circulation*, vol. 133, no. 4, pp. 447–454, 2016.

[3] V. T. Nkomo, J. M. Gardin, T. N. Skelton, J. S. Gottdiener, C. G. Scott, and M. Enriquez-Sarano, "Burden of valvular heart diseases: a population-based study," *The Lancet*, vol. 368, no. 9540, pp. 1005–1011, 2006.

[4] G. Cioffi, L. Tarantini, S. De Feo, G. Pulignano, D. Del Sindaco, C. Stefenelli, A. Di Lenarda, and C. Opasich, "Functional mitral regurgitation predicts 1-year mortality in elderly patients with systolic chronic heart failure," *European journal of heart failure*, vol. 7, no. 7, pp. 1112–1117, 2005.

[5] A. B. Goldstone, P. Atluri, W. Y. Szeto, A. Trubelja, J. L. Howard, J. W. MacArthur Jr, C. Newcomb, J. P. Donnelly, D. M. Kobrin, M. A. Sheridan *et al.*, "Minimally invasive approach provides at least equivalent results for surgical correction of mitral regurgitation: a propensity-matched comparison," *The Journal of thoracic and cardiovascular surgery*, vol. 145, no. 3, pp. 748–756, 2013.

[6] D. M. Cosgrove III, J. F. Sabik, and J. L. Navia, "Minimally invasive valve operations," *The Annals of thoracic surgery*, vol. 65, no. 6, pp. 1535–1539, 1998.

[7] L. H. Cohn, D. H. Adams, G. S. Couper, D. P. Bichell, D. M. Rosborough, S. P. Sears, and S. F. Aranki, "Minimally invasive cardiac valve surgery improves patient satisfaction while reducing costs of cardiac valve replacement and repair." *Annals of surgery*, vol. 226, no. 4, p. 421, 1997.

[8] B. Ramlawi and J. S. Gammie, "Mitral valve surgery: current minimally invasive and transcatheter options," *Methodist DeBakey cardiovascular journal*, vol. 12, no. 1, p. 20, 2016.

[9] T. Feldman, S. Kar, M. Rinaldi, P. Fail, J. Hermiller, R. Smalling, P. L. Whitlow, W. Gray, R. Low, H. C. Herrmann *et al.*, "Percutaneous mitral repair with the mitraclip system: safety and midterm durability in the initial everest (endovascular valve edge-to-edge repair study) cohort," *Journal of the American College of Cardiology*, vol. 54, no. 8, pp. 686–694, 2009.

[10] M. Y. Desai, F. Grigioni, M. Di Eusanio, M. Saccocci, M. Taramasso, F. Maisano, R. M. Suri, and A. M. Gillinov, "Outcomes in degenerative mitral regurgitation: current state-of-the art and future directions," *Progress in cardiovascular diseases*, vol. 60, no. 3, pp. 370–385, 2017.

[11] X. Hu, A. Chen, Y. Luo, C. Zhang, and E. Zhang, "Steerable catheters for minimally invasive surgery: a review and future directions," *Computer Assisted Surgery*, vol. 23, no. 1, pp. 21–41, 2018.

[12] M. Sherif, L. Paranskaya, S. Yuecel, S. Kische, O. Thiele, G. D'Ancona, A. Neuhausen-Abramkina, J. Ortak, H. Ince, and A. Öner, "Mitraclip step by step; how to simplify the procedure," *Netherlands Heart Journal*, vol. 25, no. 2, pp. 125–130, 2017.

[13] R. P. Sharma, M. Makar, and S. Kar, "An overview of the mitraclip procedure," *Journal of Structural Heart Disease*, vol. 1, no. 3, pp. 127–136, 2015.

[14] K. D. Yildirim, B. Basar, A. E. Campbell-Washburn, D. A. Herzka, O. Kocaturk, and R. J. Lederman, "A cardiovascular magnetic resonance (cmr) safe metal braided catheter design for interventional cmr at 1.5 t: freedom from radiofrequency induced heating and preserved mechanical performance," *Journal of Cardiovascular Magnetic Resonance*, vol. 21, no. 1, p. 16, 2019.

[15] K. Sreerangathama Suresh, Q. HE, D. Onohara, T. Kono, E. Sarin, and M. Padala, "Cardiac leaflet enhancer (carlen) for transcatheter repair of functional mitral regurgitation: In vitro and chronic animal feasibility studies," *Structural Heart*, vol. 4, no. sup1, pp. 76–77, 2020.

[16] R. J. J. Brockenbrough EC, Braunwald E, "Transseptal left heart catheterization: a review of 450 studies and description of an improved technic," *Circulation*, vol. 25, no. 1, pp. 15–21, 1962.

[17] Y. Kim, S. S. Cheng, and J. P. Desai, "Active stiffness tuning of a spring-based continuum robot for mri-guided neurosurgery," *IEEE Transactions on Robotics*, vol. 34, no. 1, pp. 18–28, 2017.

[18] A. Radinovic, P. Mazzone, G. Landoni, E. Agricola, D. Regazzoli, and P. Della Bella, "Different transseptal puncture for different procedures: Optimization of left atrial catheterization guided by transesophageal echocardiography," *Annals of cardiac anaesthesia*, vol. 19, no. 4, p. 589, 2016.